The Role of Photoinduced Defects in TiO_2 and Its Effects on Hydrogen Evolution from Aqueous Methanol solution

Xiaoyi Yang, Christoph Salzmann, Huahong Shi, Hongzhi Wang, Malcolm L. H. Green, and Tiancun Xiao*

Inorganic Chemistry Laboratory, University of Oxford, South Parks Road, OX1 3QR, United Kingdom, and Department of Thermal Energy Engineering, Beihang University, Beijing, 100083, P. R. China

Received: December 11, 2007; Revised Manuscript Received: August 14, 2008

The hydrogen evolution from aqueous methanol solutions was found to follow two stages of zero order kinetics during photoreactions using TiO_2 as the photocatalyst. Maximal hydrogen evolution was found at the 10% (v/v) methanol solution. X-ray photoelectron spectroscopy (XPS) shows that Ti(1566) defects are formed on the surface of TiO_2 and X-ray powder diffraction (XRD) indicates that Ti(1566) defects are also formed in the bulk after photoreaction. Formation of defects is also shown by broadening of Bragg peaks and blue shifts and peak broadening in Raman spectroscopy. The defect disorder results in the increase of hydrogen evolution. UV−vis diffuse reflection spectra confirm that new absorptions in the visible light region are related to the defect content. At high methanol concentration, XPS implies that the active sites of the surface are blocked by hydroxyl groups, which results in the decrease of hydrogen evolution. TEM images showed that the photoreaction occurred on the surface of the photocatalyst as the surface of the TiO_2 became rough after the photoreaction.

Introduction

The energy of solar radiation in the visible to ultraviolet region is of a suitable magnitude to induce transitions between electronic energy levels; thus, the heterogeneous photochemistry has attracted considerable attention in this field of solar energy utilization.[1,2] Titania (TiO_2) and TiO_2-based materials have very promising properties for uses as photocatalysts for solar hydrogen generation in terms of the considerable resistance to chemical and photochemical corrosion and reactivity with both light and water.[3,4] Anatase and rutile are the two main forms of TiO_2. The band gap of anatase is 3.23 eV (384 nm), whereas that of rutile is 3.02 eV (410 nm); hence, only UV light, merely 5% of the light from the solar spectrum, is able to create electron−hole pairs and to initiate photocatalytic processes. The photo activities of TiO_2 as a semiconductor are controlled not only by the band gap but also by the band potentials and the efficiency of the charge transfer. The relevant potential of the electron acceptor is thermodynamically required to be below the conduction band potential, and the potential of the electron donor should be above the valence band potential. As the conduction band potential of rutile is lower than the standard redox potential of H_2/H_2O, pure rutile cannot photoreduce pure water to hydrogen under the standard condition. In addition, the photoexcited electron−hole pairs require rapid transfer of charge to the active surface sites of the photocatalyst in order to restrict electron−hole pair recombination. The driving force for the electron transfer is the energy difference between the conduction band of the semiconductor and the reduction potential of the acceptor. The energy of the conduction band of the TiO_2 (E^0 (red) = −0.26 V) is quite near the reduction potential of E^0 (H^+/H_2) = 0. Consequently, the main limitations of using TiO_2 efficiently are the rapid recombination of photogenerated electron/hole pairs and the poor activation through visible light.[5]

In response to these deficiencies, most researches have focused on the modification of TiO_2-based photocatalysts including doping/implanting with metals[6,7] or nonmetals[8−10] and synthesizing composite semiconductors[11−13] in order to narrow the band gap for improving the absorption of visible light. Band gap narrowing often results in a lower energy of the conduction band or a higher energy of the valence band, and subsequently a decrease in redox activity.[14] The addition of sacrificial reagents, as electron donors, has been used to prevent rapid recombination of electron−hole pairs and backward reactions.[15,16] Most organic compounds can be oxidized by a TiO_2 photocatalyst;[17−19] therefore, many organic pollutants in wastewater can be utilized as good electron donors for photocatalytic hydrogen evolution. Accordingly, it is very practical to combine the photocatalytic production of hydrogen evolution with the degradation of pollutants.[20]

Defect formation is a main factor in changing the properties of nanoscale materials. However, some research has focused on decreasing the size of nanoscale TiO_2[21,22] and even on the defect structure of TiO_2,[23,24] but little research has studied the photoinduced defect formation of TiO_2 and its effects on photocatalyst activity. At the nanoscale level of photocatalyst, point defects and bulk defects are the main important factors to influence the properties of crystalline material. TiO_2 is a nonstoichiometric compound,[25] and oxygen vacancies and Ti(1566) interstitials can be considered the predominant defects on the surface and in the bulk of the TiO_2 particles.[24,26] Defects in semiconductors can act as shallow trapping sites, and point defects associated with surface active sites influence the effective charge transfer. The properties of TiO_2 are closely related to the defect disorder and the consequent electronic structure.[27,28]

Photoirradiation of solid can induce the formation of intrinsic and extrinsic defects through trapping of photogenerated charge

* Corresponding author. Tiancun Xiao. Address: Inorganic Chemistry Laboratory, University of Oxford, South Parks Road, OX1 3QR, U.K. Tel.: +44 1865272660; Fax: +44 1865272690. E-mail address: xiao.tiancun@chem.ox.ac.uk.

10.1021/jp804305u CCC: $40.75
Published on Web 10/04/2008

carriers and excitons.[29] Light can induce defects on surface or subsurface sites of photocatalysts. Here, we show how the photochemical reaction induced formation of defects in TiO_2 and its influences on hydrogen evolution from aqueous methanol solutions.

Experimental Section

2.1. Preparation of TiO_2 Photocatalyst. Nanoscale mesoporous TiO_2 samples were prepared by using the sol−emulsion−gel method.[22] Tetrabutyl titanate (20 g) was used as precursor and mixed with 100 mL cyclohexanol under stirring. CTAB as surfactant (0.08 g) was dissolved in 40 mL distilled water and then was added to another 100 mL cyclohexanol solution. After mixing the above solutions under mechanical agitation followed by stirring for 20 h, pH was adjusted to around 8.0 by using triethylamine as a gelling reagent. The gel particles were then separated by centrifugation at 4500 rpm and then washed with acetone. The resultant filter cake was dried in the air, and then calcined at 500 °C for 2 h.

2.2. Photocatalytic Reaction. The titania powders (200 mg) were dispersed in 100 mL methanol/water mixtures inside a Pyrex glass reactor. The reactor was then thoroughly purged with argon and sealed. After that, the suspension was irradiated from one side of the reactor with a 300 W Xe lamp (PLS-SXE300). The evolution of H_2 was measured by gas chromatography.

2.3. Sample Characterization. X-ray diffraction of the samples was carried out by an X-ray diffractometer using Cu Kα radiation. A transmission electron microscope (JEM 4000) was used for high-resolution images of the photocatalysts. The UV−vis absorption spectra were recorded with a UV−vis spectrophotometer (U-3310) equipped with a diffuse-reflectance attachment. Raman spectra were recorded using a Jobin Yvon spectrometer (Labram 1B) equipped with a microscope, through a 50-fold magnification objective (Olympus Company), by coadding four spectra with collection times of 1 s each. A 20 mW He−Ne laser (632.8 nm) was used, and the 1800 L/mm grating provides a resolution of 1.0 cm^{-1} at 200 cm^{-1}. The abscissa was calibrated with the 520.7 cm^{-1} peak of a silicon standard, and the sharp Raman shifts are accurate within the limits of the resolution. X-ray photoelectron spectrometer was performed in an ion pumped UHV chamber equipped with a VG nine channel CLAM4 electron energy analyzer. 300 W unmonochromated Mg X-ray excitation was used. The CLAM 4 has variable slits for small area analysis. The largest slit (5 mm) was used in this case with no apertures selected. The analyzer was operated at constant pass energy of 100 eV for survey scans and at 20 eV for detailed scans.

Results and Discussion

3.1. Kinetics of H_2 Evolution from Water−Methanol Solution. For TiO_2 photocatalyst, electrons are excited into the conduction bands under irradiation, leaving positively charged holes at the band edge of the valence band. Then, electrons are transferred into the empty acceptor orbital from the TiO_2 conduction band. The driving force for the heterogeneous electron transfer is the energy difference between the conduction band of the TiO_2 and the reduction potential of the acceptor. Simultaneously, electrons are donated from the filled donor orbital to recombine with the holes at the valence band edge. The driving force for the heterogeneous electron transfer is the energy difference between the valance band of the TiO_2 and the oxidation potential of the donor.

The potential of methanol oxidation by a hole to an electron-donating species $\bullet CH_2OH$ is $E^0(\bullet CH_2OH/CH_2O) = -0.95$ V[30] and to CO_2 is $E^0(CH_3OH/H_2CO_3) = 0.044$ V,[31,32] whereas the potential of water oxidation is $E^0(H_2O/O_2) = 1.23$ V. As the higher energy difference between the valence band of TiO_2 (E^0 (ox) = 2.94 V) and methanol oxidation, water oxidation was limited and the excited electrons were restricted to recombination due to positively charged hole utilization by the methanol. In additional, evolution of H_2 can be enhanced by the electron-donating species ($\bullet CH_2OH$) through a larger negative potential[33] and accordingly restriction of recombination.

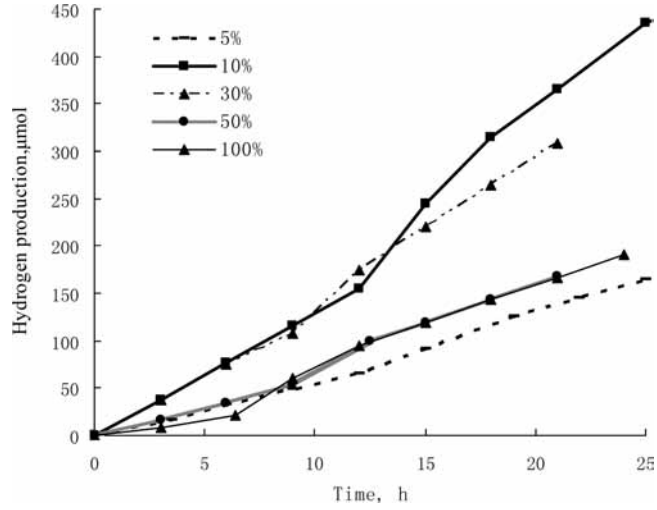

Figure 1. The effect of methanol concentration (v/v) on hydrogen evolution. The data for 50% and 100% methanol concentrations (v/v) are essentially coincidental after 12 h photoreaction.

The photocatalytic evolution of hydrogen for different methanol concentrations is shown in Figure 1.

An experiment with pure water confirmed that only an extremely minute amount of hydrogen and oxygen was generated with hydrogen and oxygen being at the stoichiometric ratio, which further confirmed water splitting. Higher efficiencies for the photoinduced hydrogen evolution can be achieved by using methanol as a sacrificial agent. As the methanol molecule competes with the water molecule to seize the hole, only traces of oxygen evolution were observed. In <30% methanol solution, formaldehyde and formic acid were identified as trace products in the liquid phase and traces of CO and CO_2 were investigated in the gas phase, which suggests that methanol is oxidized by the photogenerated hole. In >30% methanol solution, methane was investigated in the gas phase besides hydrogen and traces of CO and CO_2, which implies that methanol is reduced to methane by excited electron. In pure methanol solution (99.9%), the gas content was H_2, CH_4, CO_2, and CO, which implies that methanol is oxidized by the photogenerated hole on one hand and methanol is reduced by the excited electron on the other hand.

In pure water, water is used both as the acceptor molecule and the donor molecule; the same quality of hydrogen and oxygen were detected (Figure 2a). In methanol solution, methanol is mainly considered the donor molecule and water is the acceptor molecule to produce hydrogen. Therefore, only traces of oxygen were observed (Figure 2b). In pure methanol solution (Figure 2c), as methanol is used both as the donor molecule and the acceptor molecule, methanol was oxidized to HCOOH, HCHO, CO_2, and CO, and at the same time, methanol was reduced to methane and hydrogen.

No matter what the initial methanol concentration was, the rates of hydrogen evolution were independent of concentration of methanol at the first stage or the second stage as the reaction

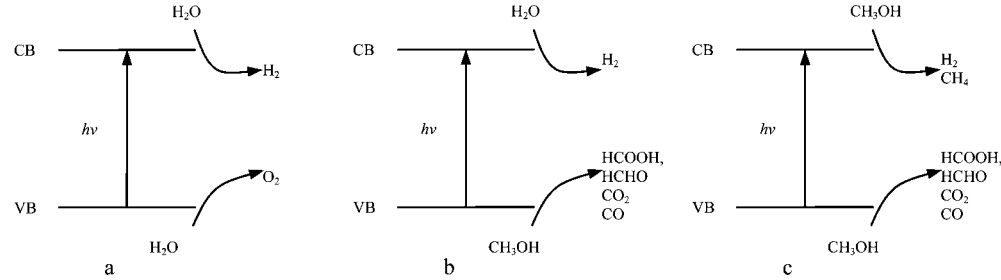

Figure 2. The photocatalytic reaction model: (a) pure water; (b) methanol solution (10%); (c) pure methanol.

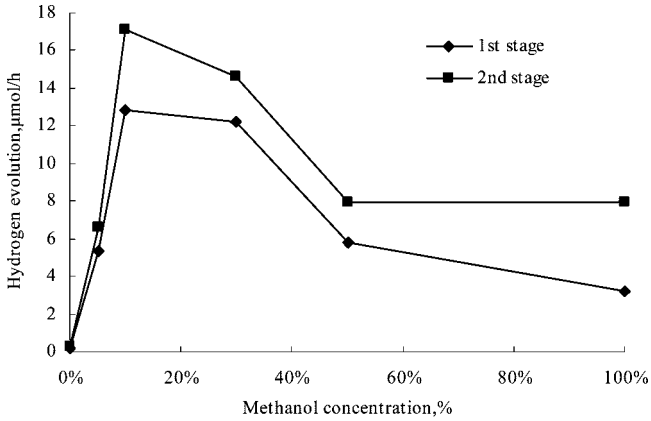

Figure 3. Hydrogen evolution rates of two stages on different methanol concentrations.

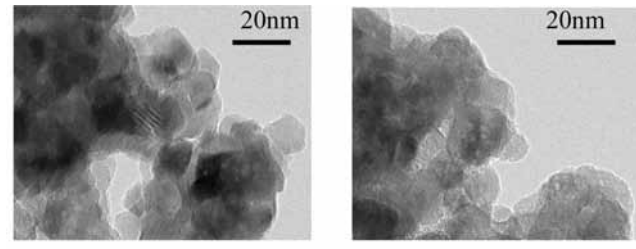

Figure 4. TEM images of TiO_2: (a) as-prepared TiO_2 and (b) TiO_2 after photoreaction.

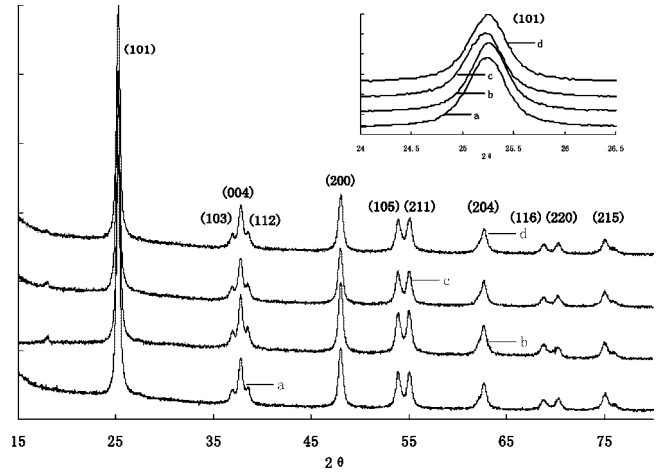

Figure 5. XRD of TiO_2 particles before and after photoreaction: (a) as-prepared TiO_2; (b) TiO_2 after photoreaction in 5% methanol solution; (c) TiO_2 after photoreaction in 10% methanol solution; (d) TiO_2 after photoreaction in 50% methanol solution.

proceeds. Therefore, kinetics analysis shows that the hydrogen evolution rates follow a two-stage zero order kinetics for all different initial methanol concentrations, given in Figure 3. The first stage, a slower reaction stage, was active for some time and then changed over to the second stage, a faster reaction stage. The retention time of the first stage was different in the different methanol concentrations. The retention time of the first stage was found to decrease with increasing methanol concentration.

The rate of hydrogen evolution was found to increase with increasing methanol concentration in the range 0−10% (v/v) and the maximal hydrogen evolution was found for the 10% methanol solution. In the range from 10% to 30% methanol solution, the rates of hydrogen evolution declined somewhat. However, the rates of hydrogen evolution decreased significantly as methanol concentration increased above 50%. The results imply that the photoreaction takes place on the surface of TiO_2, which suffers the absorption competition between methanol molecules and water molecules and the seizing competition for excited electrons.

The quantum efficiency ϕ was calculated by $\phi = 2R/I \times 100$, where R and I represent the number of evolved hydrogen molecules and the number of incident photos, respectively, and it is assumed that all incident photons are absorbed by the photocatalyst.[3] The quantum efficiencies of hydrogen evolution were 0.43% in the first stage and 0.54% in the second stage in 10% methanol solution, respectively.

The TiO_2 samples changed their colors from white to bluish gray after the photocatalytic reaction. As the crystal color of anatase is closely related to lattice imperfections, such as oxygen vacancies, Ti(1566) interstitials,[34] and the atomic ratio O/Ti,[35] this change of color implies that new defects are formed in the course of the photoreaction.

3.2. Characterization of the TiO_2 Samples. To develop an understanding of defect formation and the two-stage kinetics mechanism, TiO_2 photocatalysts were characterized before and after the photoreaction. TEM images of TiO_2 samples are given in Figure 4. The nanoscale mesoporous TiO_2 particles have been found to have an average particle size around 20 nm. The nanoscale facilitates the transfer of photogenerated electron−hole pairs to the surface, which can inhibit electron−hole recombination.[6,36] Moreover, nanoparticles of mesoporous photocatalyst that have been used here can provide more reactive sites at the surface for photocatalytic reaction due to its high specific surface area. The surface of TiO_2 tended to be coarse after the photoreaction, which suggests that the surface of the photocatalyst changes due to the photoreaction.

Powder X-ray diffraction (XRD) was employed to determine the crystalline phases present in the samples. As shown in Figure 5, all samples present mainly the anatase phase before and after the photoreactions. However, a weak peak appeared around $2\theta = 18°$ after the photoreaction in 5% and 10% methanol concentrations, which indicates the presence of small quantities of $Ti_3O_5(TiO_2 \cdot Ti_2O_3)$ phase. XRD gives evidence that the Ti(1566) formation occurred in the bulk. As the photo excitation

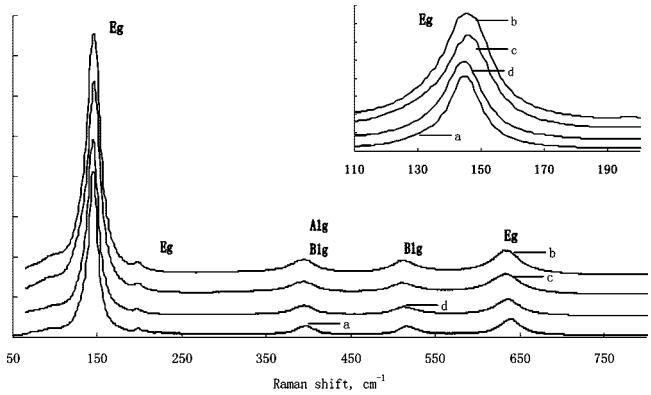

Figure 6. Raman spectra of TiO_2 samples before and after photoreaction: (a) as-prepared TiO_2; (b) TiO_2 after photoreaction in 5% methanol solution; (c) TiO_2 after photoreaction in 10% methanol solution; (d) TiO_2 after photoreaction in 50% methanol solution.

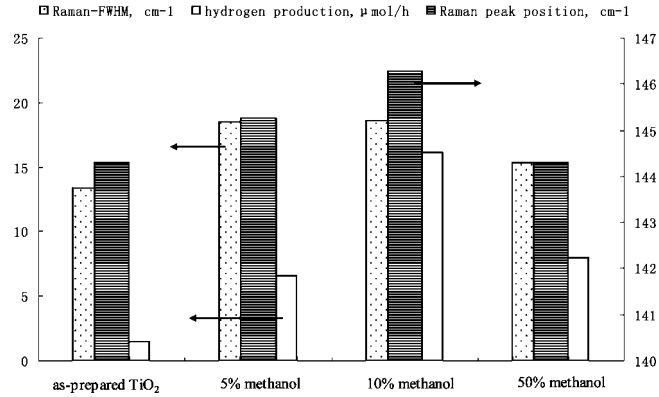

Figure 7. Raman peak shift and peak broadening before and after photoreaction.

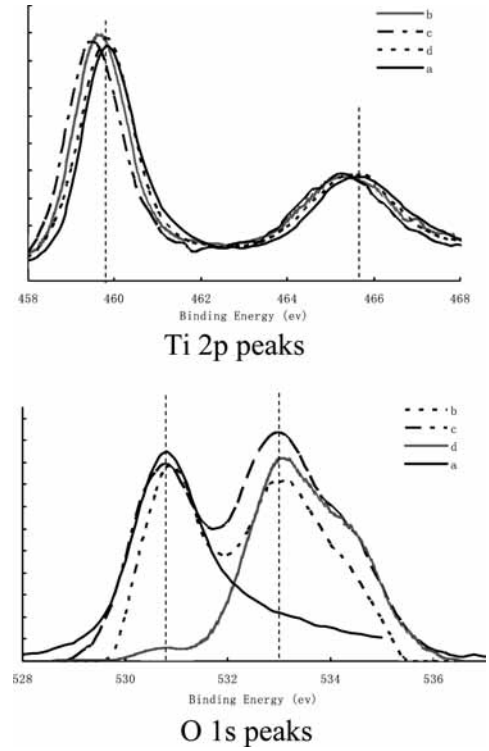

Figure 8. High-resolution XPS spectra of Ti 2p peaks and O 1s peaks of photocatalysts before and after photoreaction: (a) as-prepared TiO_2; (b) TiO_2 after photoreaction in 5% methanol solution; (c) TiO_2 after photoreaction in 10% methanol solution; (d) TiO_2 after photoreaction in 50% methanol solution.

induces electron−hole pairs, Ti(1566) defects are formed while the holes are consumed by methanol, but the excited electrons remain. Similar to Ti_2O_3 showing a violet color and Ti_3O_5 a black color, the change of color could be the result of defect formation during the photoreaction. The results also show that the rate of hydrogen evolution increases due to the formation of new defects.

According to fwhm analysis of the Bragg peak around $2\theta = 23.5°$ and by using the Scherrer equation, the average size of the as-prepared TiO_2 nanoparticles was calculated to be around 24.4 nm, which is approximately in agreement with the average particle sizes obtained from TEM. The width of XRD peaks broadened after the photoreaction, and this can be explained by defect formation, lattice strain, and the formation of amorphous layers on the surface of the particles. The largest width broadening of XRD peaks was observed in 10% methanol concentration after photoreaction, which gave the highest rate of hydrogen evolution, implying that new defects facilitate the hydrogen evolution.

Raman spectroscopy is very sensitive toward changes in the surface of the nanoscale crystalline structure. Anatase shows a tetragonal structure comprising two formula units per primitive unit cell and exhibits six Raman active modes in terms of group theory. The Raman spectra, measured before and after the photoreactions, are given in Figure 6.

The Raman spectra of the samples before and after the photoreaction show the Raman active modes of anatase,[37] which are in good agreement with the XRD results. The strongest intensity mode is around 145 cm^{-1} which is close to 144 cm^{-1} observed from a single crystal of anatase.[38] E_g modes are observed at 146, 198.5, and 635.3 cm^{-1}; a B_{1g} mode is at 396.8 cm^{-1}; and at 513.6 cm^{-1}, a doublet of the A_{1g} and B_{1g} modes is observed.

Generally, changes of the Ti/O ratio can result in Raman band shifting and changes of peak width.[39,40] Furthermore, a blue shift of the lowest-frequency E_g Raman modes is ascribed to a combined mechanism of phonon confinement and non-stoichiometry.[41] Raman peaks of anatase were found to broaden slightly and blue-shift additionally after the photocatalytic reactions (Figure 7), which indicates a change of the Ti/O ratio. As Raman spectroscopy does not show evidence for the existence of crystalline Ti_3O_5 in the samples, these results indicate that most of the Ti(1566) has entered into the matrix of mesoporous TiO_2. Actually, inner Ti(1566) can only occur at calcination above 973 K,[42−44] along with phase change from anatase to rutile, whereas Ti(1566) defects can be formed in the bulk of anatase by photoreaction at room temperature. Raman spectra showed the largest blue shift and peak broadening of TiO_2 after photoreaction in 10% methanol solution, which also implies the highest defect concentration.

TABLE 1: Binding Energies before and after Photoreaction

	Ti, eV				O 1s, eV	
sample	$2p_{1/2}$	$2p_{3/2}$	Ti 2p Peak separation, eV	Ti $2p_{1/2}$ fwhm,eV	O^{2-}	OH
TiO_2	459.8	465.6	5.8	1.04	530.8	
5% methanol	459.6	465.2	5.6	1.06	530.8	533
10% methanol	459.4	464.8	5.4	1.13	530.8	533
50% methanol	459.8	465.4	5.8	1.04		533

The chemical states of surface species on photocatalysts were measured by XPS. High-resolution XPS spectra of the Ti 2p and O 1s region are presented in Figure 8. The observed energies are summarized in Table 1.

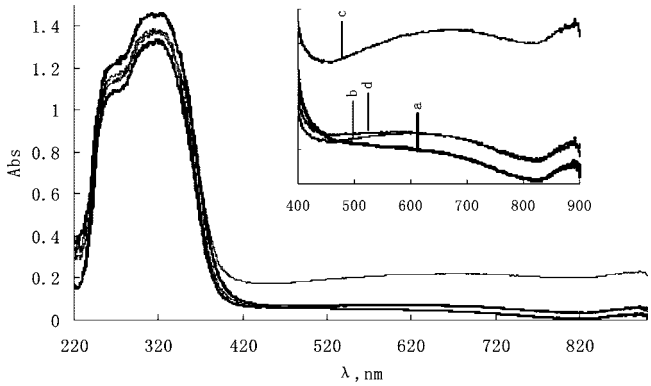

Figure 9. Diffuse reflectance spectra of TiO_2 before and after photoreaction: (a) as-prepared TiO_2; (b) TiO_2 after photoreaction in 5% methanol solution; (c) TiO_2 after photoreaction in 10% methanol solution; (d) TiO_2 after photoreaction in 50% methanol solution.

The Ti $2p_{1/2}$ and Ti $2p_{3/2}$ spin−orbital splitting photoelectrons for as-prepared TiO_2 are located at binding energies of 459.8 and 465.6 eV, respectively, as seen in Table 1. The peak separation between the Ti $2p_{1/2}$ and Ti $2p_{3/2}$ signals shortened after the photoreactions.

Atoms of a higher positive oxidation state exhibit a higher binding energy due to the extra Coulombic interaction between the photoemitted electron and the ion core. The binding energy of the Ti 2p peak moved to lower energy values, indicating reduction of Ti to a lower valence on the surface of TiO_2 as a consequence of the photoreaction. The lowest binding energy was found for the Ti 2p peak of the photocatalyst after photoreaction in 10% methanol solution, which showed a shift of 0.4 eV compared to pure TiO_2. This indicates that more Ti(1566) is present on the surface of TiO_2 after photoreaction and that more Ti(1566) defects are formed in TiO_2 after the photoreaction in 10% methanol solution, which shows the most efficient hydrogen evolution. A broader fwhm of the Ti 2p peak was also found for the photocatalyst after photoreaction in 10% methanol solution.

The O 1s curve of as-prepared TiO_2 shows only one peak located at a binding energy of 530.8 eV, indicating an O^{2-} species. However, after photoreaction in 5% and 10% methanol solution, an additional peak of O 1s was observed at about 533 eV, which was assigned to hydroxyl (OH) species on the surface of TiO_2. The photocatalyst only showed one peak for the hydroxyl species after photoreaction in 50% methanol solution. The surface of TiO_2 seems to be completely covered with hydroxyl after photoreaction in 50% methanol solution. This could be the reason that the rate of hydrogen evolution decreased with the increase of methanol concentration because the active sites on the surface have been blocked by the hydroxyl groups.

From UV−vis diffuse reflection spectra (Figure 9), it can be seen that the maximum of absorbance appears in the UV range. However, the absorption of the photocatalysts in the visible spectral region increased, and the optimal absorption of the photocatalysts in the visible spectral region was obtained after photoreaction in 10% methanol solution. Raman, XPS, and XRD spectra gave the same evidence that the highest concentration of defects appeared in the photocatalysts after photoreaction in 10% methanol solution. The Ti(1566) defects in the bulk and the surface caused the absorbance edge of TiO_2 to be shifted to the higher wavelength region. Accordingly, new absorptions in the visible light region are related to the defect content of the samples.

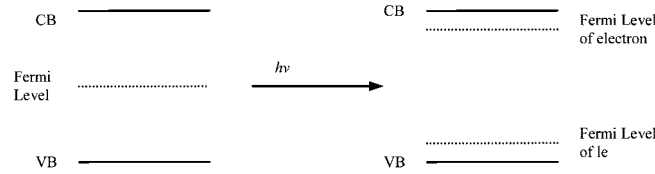

Figure 10. The Fermi level of a photocatalyst in the dark and under irradiation.

3.3. Mechanisms of Photoinduced Defects Formation. From a physical point of view, the photoexcited state of the solid is created by absorption of light quanta. The thermodynamic state in a nonirradiated ideal solid can be characterized by the position of a unique Fermi level, but the state in a photoexcited ideal solid can be depicted by two quasi-Fermi levels for electrons and holes, respectively, given in Figure 10.

Accordingly, the photocatalyst corresponds to two different thermodynamic functions with and without irradiation. The photocatalyst returns to the initial state through external charge transfer processes after the ideal photocatalytic reaction. However, a real solid photocatalyst changes its state with higher reduced or oxidized states during photoexcitation by trapping charge carriers and excitons regardless of surface photochemical redox reactions. The new states correspond to the creation of quasi-Fermi levels for the photoinduced defects, which generally differ from quasi-Fermi levels for the photogenerated electrons and holes or from Fermi level characterizing the initial state.[45] That can be confirmed by the photoinduced formation of Ti(1566) in TiO_2 photocatalyst after irradiation, and defects can be preserved after photoreaction. The photoinduced solid remains in a new metastable excited state with new defect creation. This is the reason that the states and the compositions of photocatalyst surface changed after photoreaction.

From a chemical point of view, the ideal photocatalytic reaction of hydrogen production should be that the holes involved in surface oxidation reaction equal the electrons in the surface reduction reaction. The TiO_2 photocatalyst returns to its original ground state after a closed-loop photoreaction. However, a nonideal surface reaction, the activation energy barrier for water reduction, is different from that for methanol oxidation, and the binding energy of the absorption of methanol on the surface is not the same as that of the absorption of water. Therefore, the rate of surface oxidation does not equal the rate of surface reduction. Photoinduced color centers are formed by altering the deviation of photoreaction from equality. Accordingly, excess photoadsorption of donor molecules increases the number of electron color centers, whereas excess photoadsorption of acceptor molecules increases the number of hole color centers. The more strongly the photoreaction deviates from equality, the more color centers are formed. The results from Raman, XRD, and XPS also imply that the level of defect saturation is different after photoreaction in different methanol solutions. Excess charges accumulate in the photocatalyst due to deviation of the photoreaction from equality. The more remarkable the nonideal photocatalytic reaction of the surface is, the more excess charges accumulate in the photocatalyst. Consequently, the photocatalyst changes its thermodynamic and chemical states after irradiation until the corresponding accumulation of excess charges become saturated.

Experiments have confirmed that a defect-free surface of TiO_2 is not reactive with water,[46] but the dissociation of water molecules can be enhanced by defects formed by a chemical reduction of undoped TiO_2.[47] Moreover, the photoelectrons can be trapped by Ti(1566) defects leading to the inhibition of the

electron−hole recombination. Those could explain that the hydrogen evolution followed two-stage kinetics. At the beginning of the photoreaction, the hydrogen evolution starts from the first stage. After the first stage, there is a transitional stage which is the stage for the photoinduced defect formation. Only when the photoinduced color centers become saturated, do the thermodynamic state and the chemical composition of the photocatalyst reach the stationary states, and accordingly the rate of hydrogen evolution showed the second stage.

In a photocatalytic process, the reduction reagent should chemisorb on the photocatalytic surface long enough for absorbate molecules to undergo chemical transformation, but at the same time, the reaction products on the surface should easily desorb under ambient conditions with the consequence of releasing the active centers for the next photoreaction. In higher concentrations of methanol solution, hydroxyl groups remained on the surface of photocatalysts and subsequently blocked the active sites. That could be the reason that the maximal hydrogen evolution was found at only 10% methanol solution but not at higher concentrations of methanol solution.

Conclusion

Higher efficiencies for the photoinduced hydrogen evolution can be achieved by using methanol as a sacrificial agent, and maximal hydrogen evolution was found at 10% methanol solution. In pure methanol solution (99.9%), the content of gases was H_2, CH_4, CO_2, and CO, which implies that methanol was oxidized by a hole on one hand and methanol was reduced by an excited electron on the other hand.

The photochemical properties of TiO_2 are related closely to the photoinduced defect formation, which results in two-stage zero order kinetics of hydrogen evolution in aqueous methanol solutions. Raman, XPS, and XRD spectra gave the same evidence that the highest concentration of defects appeared in the photocatalysts after photoreaction in 10% methanol solution.

The photoinduced defects associated with Ti(1566) formed on the surface and in the bulk of TiO_2, which related to the active sites and thus a higher efficiency of hydrogen evolution.

Photoinduced defects in TiO_2 result in visible light absorption, which implies that the photoinduced TiO_2 remains in a new metastable state with creation of new defects.

Acknowledgment. This work was financed by the China Scholarship Council and Oxford Catalyst Center.

References and Notes

(1) Sandro, U.; Alessandro, D.; Domenica, S.; Silvia, B.; Adriano, Z.; Carlo, L. *J. Am. Chem. Soc.* **2007**, *10*, 2822.
(2) Masaaki, K.; Masaya, M.; Michio, U.; Masakazu, A. *Appl. Catal. A* **2007**, *325*, 1.
(3) Zhigang, Z.; Jinhua, Y.; Kazuhiro, S.; Hironori, A. *Nature* **2001**, *6*, 625.
(4) Daling, L.; Tsuyoshi, T.; Nobuo, S.; Yasunobu, I.; Kazunari, D. *Nature* **2006**, *440*, 295.
(5) Meng, N.; Michael, K. H.; Leung.Dennis, Y. C.; Leung, K. *Sumathy Renew. Sust. Energ. Rev.* **2007**, *11*, 401.
(6) Dengwei, J.; Yaojun, Z.; Liejin, G. *Chem. Phys. Lett.* **2005**, *415*, 74.
(7) Teruhisa, O.; Fumihiro, T.; Kan, F.; Shinobu, I.; Michio, M. *J. Photochem. Photobiol. A* **1999**, *127*, 107.
(8) Hiroshi, I.; Yuka, W.; Kazuhito, H. *J. Phys. Chem. B* **2003**, *107*, 5483.
(9) Asahi, R.; Morikawa, T.; Ohwaki, T.; Aoki, K.; Taga, Y. *Science* **2001**, *293*, 269.
(10) Khan, S. U. M.; Al-Shahry, M.; Ingler, W. B. *Science* **2002**, *297*, 2243.
(11) So, W. W.; Kim, K. J.; Moon, S. J. *Int. J. Hydrogen Energy* **2004**, *29*, 229.
(12) De, G. C.; Roy, A. M.; Bhattacharya, S. S. *Int. J. Hydrogen Energy* **1996**, *21*, 19.
(13) Keller, V.; Garin, F. *Catal Commun.* **2003**, *4*, 377.
(14) Mrowetz, M.; Balcerski, W.; Colussi, A. J.; Hoffmann, M. R. *J. Phys. Chem. B* **2004**, *108*, 17269.
(15) Sang Gi, L.; Sangwha, L.; Ho.In, L. *Appl. Catal. A* **2001**, *207*, 173.
(16) Ryu Abe Kazuhiro, S.; Hironori, A. *Chem. Phys. Lett.* **2003**, *379*, 230.
(17) Chatterjee, D.; Dasgupta, S. *J. Photochem. Photobiol.* **2005**, *6*, 186.
(18) Legrini, O.; Oliveros, E.; Braun, A. M. *Chem. Rev.* **1993**, *93*, 671.
(19) Carp, O.; Huisman, C. L.; Reller, A. *Prog. Solid State Chem.* **2004**, *32*, 33.
(20) Alexia, P.; Dimitris, I. K.; Xenophon, E. V. *Catal. Today* **2007**, *124*, 94.
(21) Yunhua, Ch.; An, L.; Fuxing, G. *Powder Technol.* **2006**, *167*, 109.
(22) Wuyi, Zh.; Qingyun, C.; Shaoqiu, T. *Powder Technol.* **2006**, *168*, 32.
(23) Nowotny, J.; Bak, T.; Nowotny, M. K.; Sheppard, L. R. *J. Phys. Chem. B* **2006**, *110*, 18492.
(24) Bak, T.; Nowotny, J.; Rekas, M.; Sorrell, C. C. *J. Phys. Chem. Solids* **2003**, *64*, 1069.
(25) Bak, T.; Nowotny, J.; Rekas, M; Sorrell, C. C. *J. Phys. Chem. Solids* **2003**, *64*, 1043.
(26) Wang, C.-C.; Jackie, Y. *Chem. Mater.* **1999**, *11*, 3113.
(27) Bak, T.; Nowotny, J.; Rekas, M.; Sorrell, C. C. *J. Phys. Chem. Solids* **2003**, *64*, 1057.
(28) Nowotny, J.; Sorrell, C. C.; Bak, T.; Sheppard, L. R. *Solar Energy* **2005**, *78*, 593.
(29) Emeline, A.; Kataeva, G.; Panasuk, A.; Ryabchuk, V.; Sheremetyeva, N.; Serpone, N. *J. Phys. Chem. B* **2005**, *109*, 5175.
(30) Nguyen, V. N. H.; Amal, R.; Beydoun, D. *Chem. Eng. Sci.* **2003**, *58*, 4429.
(31) Pei-wen, P. *Yuwen, Ch., Catal. Commun.* **2007**, *8*, 1546.
(32) Yahaya, A. H.; Gonal, M. A.; Hameed, A. *Chem. Phys. Lett.* **2004**, *400*, 206.
(33) Patsoura, A.; Kondarides, D. I.; Verykios, X. E. *Appl. Catal. B* **2006**, *64*, 171.
(34) Sekiya, T.; Ichimura, K.; Igarashi, M.; Kurita, S. *J. Phys. Chem. Solids* **2000**, *61*, 1237.
(35) Straumanis, M. E.; Ejima, T.; James, W. J. *Acta Crystallogr.* **1961**, *14*, 493.
(36) Takahara, Y.; Konde, J. N.; Takata, T. *Chem. Mater.* **2001**, *13*, 1194.
(37) Du, Y. L.; Deng, Y.; Zhang, M. S. *J. Phys. Chem. Solids* **2006**, *67*, 2405.
(38) Lottici, P. P.; Bersani, D.; Braghini, M.; Montenero, A. *J. Mater. Sci.* **1993**, *28*, 177.
(39) Parker, J. C.; Siegel, R W. *J. Mater. Res.* **1990**, *5*, 1246.
(40) Parker, J. C.; Siegel, R W. *Appl. Phys. Lett.* **1990**, *57*, 943.
(41) Zhang, W. F.; He, Y. L.; Zhang, M. S.; Yin, Z.; Chen, Q *J. Phys. D: Appl. Phys* **2000**, *33*, 912.
(42) Kongkiat, S.; Piyasan, P.; Bunjerd, J. *Appl. Surf. Sci.* **2007**, *253*, 3849.
(43) Howe, R. F.; Gratzel, M. *J. Phys. Chem.* **1985**, *89*, 4495.
(44) Lee, S. K.; Robertson, P. K. J.; Mills, A.; McStay, D.; Elliott, N.; McPhail, D. *Appl. Catal., B* **2003**, *44*, 173.
(45) Amy, L. L.; Guangquan, L.; John, T. *Chem. Rev.* **1995**, *95*, 735.
(46) Lo, W. J.; Chung, Y.; Samorjai, W. *Surf. Sci.* **1978**, *71*, 199.
(47) Kowalski, J. M.; Johnson, K. H.; Tuller, H. L. *J. Electrochem. Soc.* **1980**, *127*, 1969.

JP804305U